Potential-induced degradation of $Cu(In,Ga)Se_2$ can occur by shunting the front i-ZnO and by damaging the p-n junction

Christopher P. Muzzillo,* Kent Terwilliger, Peter Hacke, Helio R. Moutinho, Matthew R. Young, Stephen Glynn, Bart Stevens, Ingrid L. Repins, and Lorelle M. Mansfield

*Corresponding author
National Renewable Energy Laboratory, 15013 Denver W Pkwy, Golden, CO 80401, USA

Highlights

- We encapsulate laboratory CIGS cells to study field-relevant PID
- K-rich borosilicate glass reduces PID, relative to Na-rich soda-lime glass
- Stressing cells at short-circuit leads to faster PID than open-circuit
- Front-glass stress shunts the i-ZnO buffer, slowly reducing the FF
- Back-glass stress drives Na^+ into the p-n junction to rapidly degrade V_{OC} and FF

Abstract
In this work we test field-relevant potential-induced degradation (PID) behavior by encapsulating laboratory $Cu(In,Ga)Se_2$ (CIGS) solar cells and applying +1000 V uniformly on the face of the front glass. In this configuration, we find that K-rich borosilicate glass reduces the extent of PID relative to Na-rich soda-lime glass. We also find that the standard testing protocol of stressing cells at short-circuit leads to faster PID than stressing cells at open-circuit. We characterize two types of CIGS PID: The first, front shunting PID, is driven by front-glass stress and occurs when alkali metal cations accumulate in the i-ZnO buffer, where they increase shunt conductance to reduce fill factor. The second, p-n junction PID, results from back-glass stress as alkali metal cations pile up near the CIGS surface/CdS buffer, where they reduce charge carrier concentration, open-circuit voltage, and fill factor to degrade efficiency ~160 times faster than front shunting PID.

Keywords: photovoltaics, reliability, thin-film, potential-induced degradation, chalcopyrite, $Cu(In,Ga)Se_2$

1. Introduction

Potential-induced degradation (PID) occurs in fielded photovoltaic (PV) modules, particularly in modules that are strung together in series. Toward the negative end of strings, very large potentials drive alkali metal cations (primarily Na^+) into the semiconductor layers, where they eventually lead to degradation (Weber et al., 2013; Weber et al., 2017). For $Cu(In,Ga)(Se,S)_2$ (CIGS), PID occurs when alkali metal cations such as Na^+ are driven from the substrate glass or cover glass into the device. These cations can then degrade performance by compensating or shunting within the solar cell, which typically reduces its open-circuit voltage and fill factor (Yilmaz et al., 2022). The amount of Na^+ that migrates through the glass and into the device is related to the leakage current (Hoffmann and Koehl, 2014; Lechner et al., 2013; Lechner et al., 2012; Walter, 2015), so reducing the conductivity of the glass and encapsulant can reduce PID. For example, ionomer encapsulant is less conductive than poly(ethylene-vinyl acetate) (EVA), so it diminishes PID by reducing the amount of Na^+ arriving from the cover glass (Kapur et al., 2015; Yamaguchi et al., 2015). Glasses with reduced Na content also have

Pursuant to the DOE Public Access Plan, this document represents the authors' peer-reviewed, accepted manuscript. The published version of the article is available from the relevant publisher.

reduced PID because less current leaks through them (Fjällström et al., 2013; Kambe et al., 2013; Muzzillo et al., 2019; Muzzillo et al., 2018). The Na^+ pathway also matters: Lateral transport of Na^+ driven by a metal frame at the module's edge was found to be negligible (Boulhidja et al., 2017; Boulhidja et al., 2020; Voswinckel et al., 2020), while Na^+ driven from the front and back glass causes PID in CIGS, with the latter being more damaging (Alonso-Garcia et al., 2019; Mansfield et al., 2017; Muzzillo et al., 2018; Voswinckel et al., 2020). Diffusion barriers and differences in the Mo layer can also change back PID behavior (Muzzillo et al., 2019; Salomon et al., 2019; Vermang et al., 2014) while not modifying the leakage current.

Since Na^+ is hygroscopic, moisture accelerates PID by causing transparent conductive oxide (TCO) corrosion (Luo et al., 2017; Theelen and Daume, 2016). In particular, old CIGS modules have shown visible TCO corrosion resulting from PID (Hacke et al., 2015; Xiong et al., 2011), but better encapsulation can eliminate this in newer modules by eliminating moisture ingress (Hacke et al., 2015). Therefore, to correlate field PID with laboratory studies (Sakurai, K. et al., 2018), moisture should be eradicated. For our work we have developed methods that allow our small area solar cells to be encapsulated against moisture (Contreras et al., 2016; Mansfield et al., 2021), stressed, and then cored for characterization after they have degraded (Moutinho, H. R. et al., 2018; Moutinho, H.R. et al., 2018).

Partial recovery of CIGS PID has been widely documented, and can be achieved by reversing PID polarity (Alonso-Garcia et al., 2019; Boulhidja et al., 2017; Fjällström et al., 2015; Mansfield et al., 2017; Vermang et al., 2014; Weber et al., 2017), light soaking (Sakurai et al., 2019), allowing devices to sit in the dark at room temperature (Fjällström et al., 2015; Lee et al., 2021), and etching/redepositing the buffer (Fjällström et al., 2015). Theelen noted that multiple degradation mechanisms in CIGS devices can be superimposed (Theelen and Daume, 2016), and the pervasiveness of partially reversible PID indicates that recovery and degradation can also superimpose: In particular, the interruption of PID stress for characterization can affect degradation (Manz et al., 2014; Muzzillo et al., 2019). Light and electrical bias can reverse PID or prevent it from occurring in the first place (Sakurai et al., 2016, 2017; Sakurai, Keiichiro et al., 2018), so laboratory procedures should be carefully controlled to avoid test-specific degradation. Indeed, the standard for testing crystalline Si-based modules is to perform PID stress in the dark at short-circuit (International Electrotechnical Commission (IEC) 62804-1 (Luo et al., 2017)), conditions which clearly lead to test-specific PID in CIGS (Sakurai, Keiichiro et al., 2018).

To alleviate these complications, in this work we eliminate moisture effects, keep stress interruption procedures constant for all samples, account for degradation due to thermal effects alone, avoid unintended electric fields in our test chamber (Carolus et al., 2020; Luo, Wei et al., 2018), and compare results for front and back PID to better understand universal PID mechanisms. We find that using K-rich borosilicate glass (BSG) reduces front PID, relative to Na-rich soda-lime glass (SLG). We also find that the standard testing protocol of stressing cells at short-circuit (SC) leads to faster PID than open-circuit (OC). Our former work showed that back PID results from Na^+ pileup at the CIGS front surface and CdS buffer, where initial degradation is associated with a reduction in carrier concentration, open-circuit voltage (V_{OC}) and fill factor (FF). On the other hand, this work shows that front PID is much slower and results from Na^+ accumulation in the i-ZnO buffer, with a decrease in shunt resistance and FF occurring alongside the initial degradation.

2. Experimental

Pursuant to the DOE Public Access Plan, this document represents the authors' peer-reviewed, accepted manuscript. The published version of the article is available from the relevant publisher.

We previously developed a patterning procedure that allows us to encapsulate our standard small area CIGS solar cells while still permitting electrical probing with external leads (Contreras et al., 2016), where encapsulation allows us to eliminate moisture effects (more details on our reliability testing procedures are in (Mansfield et al., 2021)). Mo back contacts were sputtered onto soda-lime glass (SLG; baseline) or potassium-rich borosilicate glass (BSG). CIGS was grown by 3-stage co-evaporation at 600 °C with overall molar compositions of Cu/(Ga+In) ~ 0.85 and Ga/(Ga+In) ~ 0.3, as confirmed by X-ray fluorescence. CdS buffers were grown by chemical bath deposition in a bath set to 65 °C. Intrinsic ZnO buffer and aluminum-doped ZnO were then sputtered without intentional substrate heating. Ni/Al grids were e-beam evaporated through finger grid masks, followed by photolithographic masking of the 0.42 cm^2 device mesas and etching for isolation. Current density-voltage (JV) measurements were performed on a temperature-controlled stage at 25 °C under a xenon arc lamp calibrated to 1 sun AM1.5G with a standard Si solar cell. Extra contact shadowing was needed for the external leads, reducing current density by 6.2%. Shading from the external leads reduces efficiency by about 1.0%, so if anti-reflective coating was used instead of encapsulation, a ~2% absolute efficiency boost would be expected. Capacitance-voltage (CV) was measured at room temperature in the dark at 10 kHz, 50 mV AC voltage, DC bias from +0.6 V to -1.5 V, and carrier concentration was extracted using a dielectric constant of 13.6.

In lieu of performing stress at 85 °C and high relative humidity (RH), in which case the uniformity of the electric field over the sample face can be difficult to control, we use 10% RH and apply high voltage bias with Al foil against the back or front glass (Hoffmann and Koehl, 2014). The samples were first held at 85 °C for 24 h in order to isolate initial changes due to thermal effects alone (Muzzillo et al., 2018). Next, high voltage stress was applied at 85 °C with Al foil on the front glass at +1000 V and the cells grounded at short-circuit (SC). Thermal control samples were left at open-circuit (OC) and experienced the 85 °C with no high voltage stress. Another sample received the high voltage stress with the cells at OC (the TCO contact was grounded and the Mo contact was not probed). The stress was interrupted at 100 h, 200 h or 300 h intervals to monitor degradation by performing JV and CV. All samples were stressed and characterized in parallel, so despite the fact that the stress interruptions themselves affect degradation (Manz et al., 2014; Muzzillo et al., 2019), relative comparisons among the samples should be valid. 6 SLG baseline, 13 SLG SC, 7 SLC OC, 5 BSG baseline, 12 BSG SC, and 7 BSG OC cells were stressed. After 1640 h the stress was stopped and the samples were cored by drilling into the glass with a hollow bit. A metal handle was then bonded to the core with epoxy. Next, the sample was placed on a hotplate (65 °C) to soften the EVA, and torque was applied to the metal handle. This led to delamination at the ZnO/EVA interface (Moutinho, H. R. et al., 2018; Moutinho, H.R. et al., 2018). Secondary ion mass spectrometry (SIMS) was then performed on the exposed glass/Mo/CIGS/CdS/i-ZnO/Al:ZnO. The Na and K content in the ZnO and CIGS layers was quantified using SIMS standards.

3. Results

3.1. Na-rich SLG vs K-rich BSG

Foil on the front glass was held at +1000 V to drive alkali metal cations from the front glass into the grounded cells. A standard Na-rich SLG was compared with K-rich BSG, the latter of which led to comparable initial performance (Table 1), in line with previous work (Muzzillo et al., 2018). To track PID, the efficiency after a given stress time (η_{PID}) was divided by initial

Pursuant to the DOE Public Access Plan, this document represents the authors' peer-reviewed, accepted manuscript.
The published version of the article is available from the relevant publisher.

efficiency (before the stress began, $\eta_{PID,0}$). This quantity ($\eta_{PID}/\eta_{PID,0}$) was then divided by the corresponding scaled efficiency for the control sample that was exposed to 85 °C but not high voltage stress ($\eta_{ctrl}/\eta_{ctrl,0}$). The resulting mean data are shown for the SLG and BSG samples in Fig. 1. After 1640 h of stress, the SLG samples had degraded to less than 50% of their initial performance, while the BSG samples exhibited no degradation. The K-rich BSG leads to enough out-diffusion of K during absorber growth such that initial alkali metal concentration and efficiency are similar to the SLG baseline (despite K apparently being less active at increasing carrier concentration (Table 1)). On the other hand, the BSG conducts less leakage current via alkali metal cation transport, so PID is reduced relative to SLG. The relative behavior of SLG and BSG for front glass stress are in line with our former studies on back-glass PID (Muzzillo et al., 2019; Muzzillo et al., 2018).

Table 1. Initial photovoltaic performance for the different glasses (after 24 h thermal equilibration at 85 °C): Efficiency, V_{OC}, short-circuit current density (J_{SC}), and FF, with carrier concentration by CV and alkali metal concentration by SIMS (Na for SLG and K for BSG).

Glass	# of cells	Eff. (%)	V_{OC} (mV)	J_{SC} (mA/cm^2)	FF (%)	Carrier conc. ($\cdot 10^{16}$ cm^{-3})	Na or K conc. ($\cdot 10^{19}$ cm^{-3})
SLG	26	13.9(11)	675(14)	28.8(10)	71.7(52)	2.08(78)	1.79(44)
BSG	24	13.8(6)	651(7)	30.1(7)	70.4(33)	0.96(27)	2.61(146)

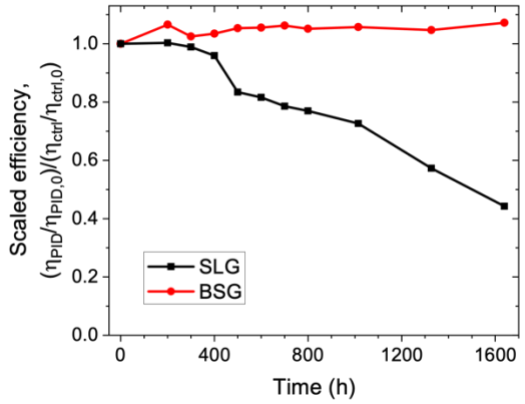

Fig. 1. Efficiency (η_{PID}) scaled to initial efficiency ($\eta_{PID,0}$) and scaled control efficiency ($\eta_{ctrl}/\eta_{ctrl,0}$) as a function of duration of high voltage applied to the front face for SLG (black squares) and BSG (red circles). The more conductive Na-rich SLG exhibits much faster front PID than the less conductive K-rich BSG. Data are for stress with cells at SC.

3.2. Front vs back PID

Applying +1000 V to the front glass in this study required 1640 h of stress to degrade the SLG samples to 44% of their initial efficiency, whereas similar degradation occurred in just 10 h when the high voltage was applied to the back glass of similar samples (Muzzillo et al., 2019). A straightforward reason for front PID being slower than back PID is that the former has the added electrical resistance of the EVA encapsulant, but this is not the only difference. Fig. 2 shows that the SLG sample degraded by front PID did not have higher Na content in the absorber than the

Pursuant to the DOE Public Access Plan, this document represents the authors' peer-reviewed, accepted manuscript.
The published version of the article is available from the relevant publisher.

control, while the back PID sample had much higher Na near the p-n junction (CIGS surface/CdS). On the other hand, the front PID sample had higher Na in the ZnO than the control (Fig. 3), while the back PID sample had lower Na in the ZnO than its control (Fig. 4). In conclusion, front PID is associated with Na accumulation in the ZnO, while back PID is associated with Na accumulation near the CIGS surface/CdS.

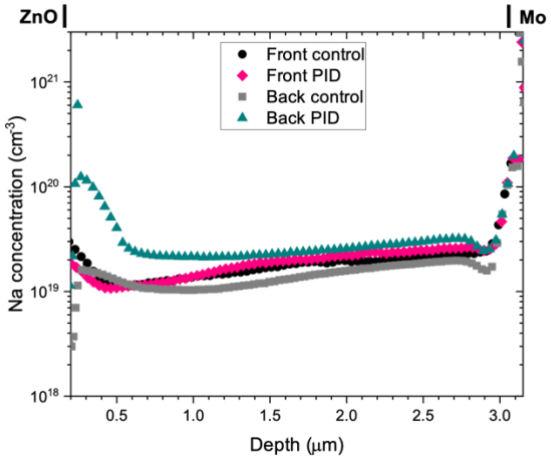

Fig. 2. Na concentration in the CIGS absorber by SIMS, shown for the front control (black circles), front PID (pink diamonds), back control (gray squares), and back PID (teal triangles). Only the back PID sample had increased Na in the absorber. Data are for SLG samples stressed with cells at SC.

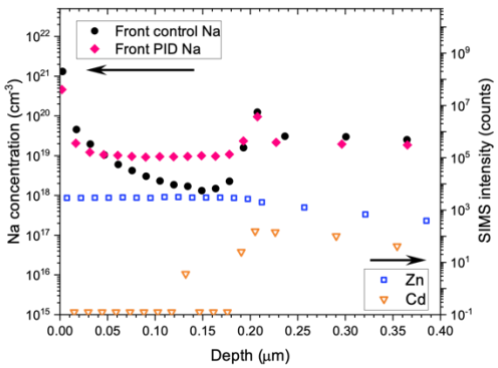

Fig. 3. Na concentration (left axis) in the ZnO layer after stress for the front control (black circles) and front PID (pink diamonds), along with SIMS intensities (right axis) for Zn (blue squares) and Cd (orange triangles), showing that front PID was associated with increased Na in the ZnO. Data are for SLG samples stressed with cells at SC.

Pursuant to the DOE Public Access Plan, this document represents the authors' peer-reviewed, accepted manuscript.
The published version of the article is available from the relevant publisher.

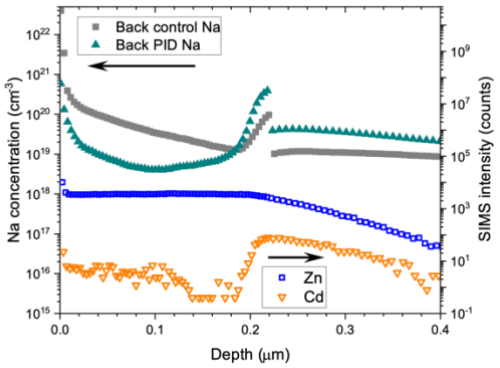

Fig. 4. Na concentration (left axis) in the ZnO layer after stress for the back control (gray squares) and back PID (teal triangles), along with SIMS intensities (right axis) for Zn (blue squares) and Cd (orange triangles), showing that back PID was associated with decreased Na in the ZnO. Data are for SLG samples stressed with cells at SC.

In agreement with former work on CIGS PID (Yilmaz et al., 2022), the loss in efficiency associated with front and back PID was correlated with V_{OC} and FF loss (but not J_{SC}). Fig. 5 shows that for front PID, a decrease in η corresponded with FF loss more than V_{OC} loss. For back PID on the other hand, η loss was more strongly associated with a decrease in V_{OC} than in FF. Previous work also associated the initial loss in back PID V_{OC} with a reduction in carrier concentration (Muzzillo et al., 2019; Muzzillo et al., 2018).

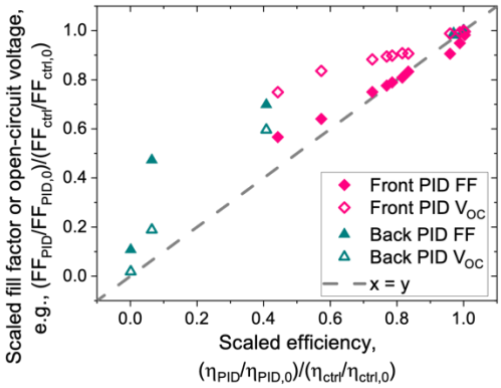

Fig. 5. Scaled FF (filled symbols) or V_{OC} (empty symbols) as a function of scaled η for front PID (pink diamonds) and back PID (teal triangles), showing that there was a stronger correlation between FF and η for front PID, while for back PID, V_{OC} correlated more with η. Data are for SLG samples stressed with cells at SC, and the dashed line is where x = y.

To further probe the difference between front and back PID, diode parameters were extracted from the dark and light JV data (Hegedus and Shafarman, 2004). The front SLG samples' diode parameters (shunt conductance, series resistance, saturation current density, and ideality factor) after 300 h of stress were scaled to their initial values and the analogous scaled control values. This procedure was repeated for 3 h of stress on the back SLG samples. These stress durations were chosen because they exhibited the onset of PID while retaining well-behaved JV characteristics (1.1% and 3.9% degradation in the front and back PID samples'

Pursuant to the DOE Public Access Plan, this document represents the authors' peer-reviewed, accepted manuscript.
The published version of the article is available from the relevant publisher.

efficiency, respectively). The complete diode parameter results are in Fig. S1 – S11. The only significant difference was in the shunt conductance: Fig. 6 and 7 show that front PID is associated with increased shunt conductance in the dark and light more than back PID.

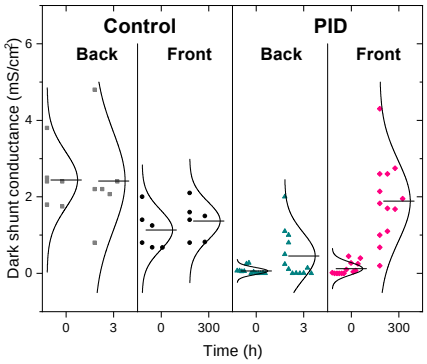

Fig. 6. Dark shunt conductance for back control (gray squares), front control (black circles), back PID (teal triangles), and front PID (pink diamonds) as a function of stress time, showing that front PID is associated with shunting more than back PID. Lines show normal distributions and means. Data are for SLG samples stressed with cells at SC.

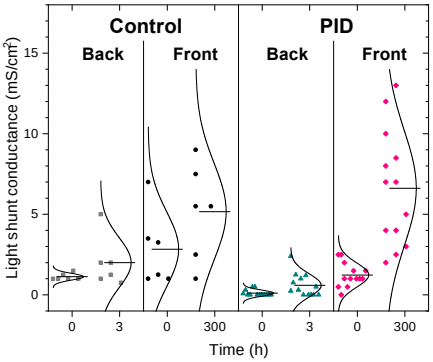

Fig. 7. Light shunt conductance for back control (gray squares), front control (black circles), back PID (teal triangles), and front PID (pink diamonds) as a function of stress time, showing that front PID is associated with shunting more than back PID. Lines show normal distributions and means. Data are for SLG samples stressed with cells at SC.

For CIGS, we have now characterized two distinct PID mechanisms: (1) Front shunting PID, which is caused by applying +1000 V to the front glass and slowly decreases FF in the absence of moisture, and (2) p-n junction PID, which is driven by applying +1000 V to the back glass and rapidly decreases carrier concentration, V_{OC} and FF in the absence of moisture. Front shunting results from alkali metal cations gathering in the i-ZnO buffer to increase shunt conductance. P-n junction PID is due to the accumulation of alkali metal cations near the junction, where they apparently compensate majority carriers to reduce the built-in field and V_{OC}; the cations may also act as shunt paths through the junction to reduce FF. If back PID experiments are performed on unencapsulated CIGS, then more Na can be drawn into the ZnO as it reacts with moisture (Salomon et al., 2019; Xiao et al., 2019), changing the degradation mechanism.

Pursuant to the DOE Public Access Plan, this document represents the authors' peer-reviewed, accepted manuscript.
The published version of the article is available from the relevant publisher.

Two prevalent kinds of PID affecting electrical performance have also been identified for crystalline Si: (1) Na^+ can accumulate at dislocations to shunt the p-n junction, decreasing FF but leaving V_{OC} and J_{SC} relatively unchanged (shunting PID) (Colli, 2013; Naumann et al., 2014b), and (2) Na^+ can accumulate near the Si_xN_y or AlO_x layers, where they neutralize the desired negative fixed charge to reduce the carrier selectivity of contact layers, decreasing J_{SC} and V_{OC} but not FF (polarization PID) (Luo, W. et al., 2018; Naumann et al., 2014a). We note that PID related to the accumulation of anions has also been documented in CIGS (Sakurai et al., 2019) and Si (Swanson et al., 2005). In summary, for crystalline Si and CIGS an important segment of PID mechanisms involves drifting of alkali metal cations from the glass toward the device. Depending on their particular distribution, these cations then degrade through charge accumulation or shunting. Thus, simple (Muzzillo et al., 2019) and more sophisticated (Schulze et al., 2020) mass balance models that account for Na^+ drift and diffusion can describe degradation kinetics.

3.3. Stress with cells at SC vs OC

The IEC 62804-1 standard for laboratory PID testing of crystalline Si PV modules dictates that they be held at SC in the dark with various options for temperature, relative humidity and duration (Luo et al., 2017). The standardized testing protocols for thin-film modules are still being developed. As noted in the introduction section, light and electrical bias affect CIGS PID, so cells/modules held at SC in the dark are expected to exhibit test-specific degradation. Since illuminating samples during PID stress adds substantial cost and complexity to the environmental stress chamber, finding an electrical bias condition that can substitute for light would be a more convenient means to emulate field conditions in laboratory tests. We previously found that leaving cells at OC slowed back PID, and Fig. 8 shows that this trend holds for front PID as well. We hypothesize that in both cases, OC slows PID relative to SC by restricting the free motion of Na^+ so that it accumulates less near the vulnerable p-n junction (for back PID) and in the i-ZnO buffer (for front PID; see schematic in Fig. 9). In the future, confirming the differences and similarities between OC stress in the dark and field PID may inform more appropriate testing standards.

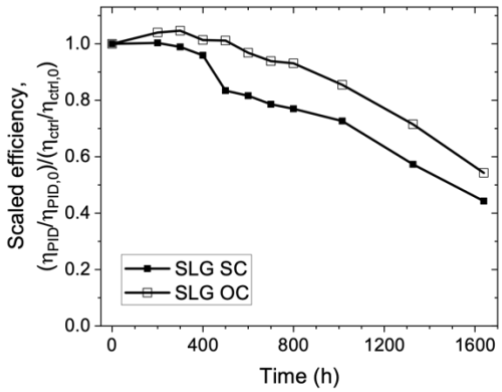

Fig. 8. Efficiency (η_{PID}) scaled to initial efficiency ($\eta_{PID,0}$) and scaled control efficiency ($\eta_{ctrl}/\eta_{ctrl,0}$) as a function of time of +1000 V applied to the front glass for cells stressed at SC

Pursuant to the DOE Public Access Plan, this document represents the authors' peer-reviewed, accepted manuscript.
The published version of the article is available from the relevant publisher.

(filled squares) and OC (empty squares). The OC leads to slower PID. Data are for SLG samples comprising 13 SC, 7 OC and 6 control solar cells.

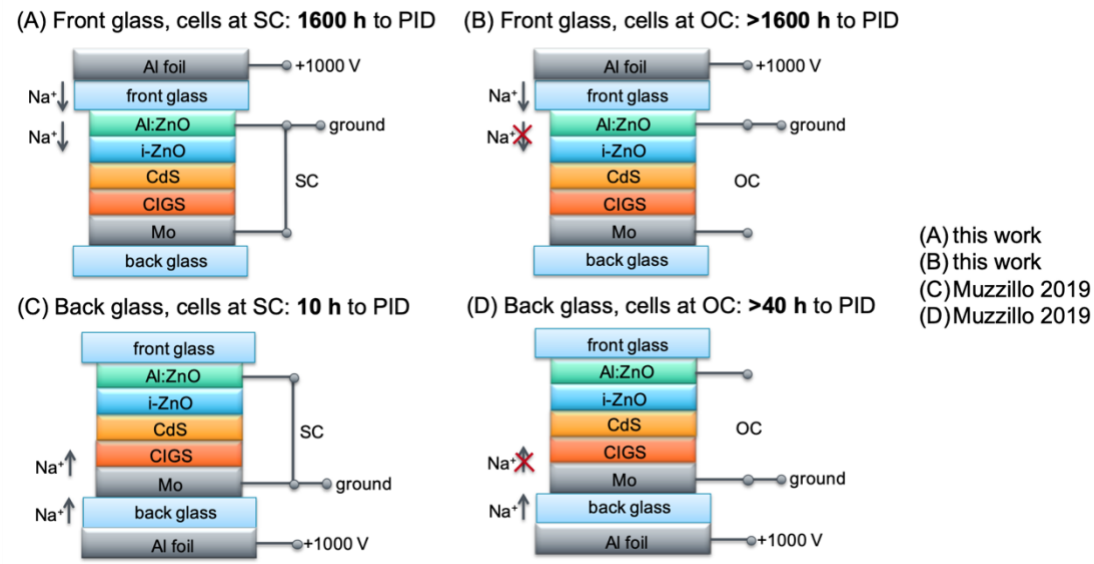

Fig. 9. Schematic showing the laboratory testing configuration and time to PID for (A) front PID at SC, (B) front PID at OC, (C) back PID at SC, and (D) back PID at OC. We hypothesize that OC slows PID relative to SC in both cases as a result of restricted Na^+ transport. Layer thicknesses are not to scale.

4. Conclusions

In this work we account for the factors that complicate CIGS PID in the laboratory: We eliminate moisture, isolate PID with thermal control samples, and stress and test duplicate samples in parallel to keep PID reversal during characterization consistent. Using these methods we characterized two types of CIGS PID: (1) Front shunting PID, which is driven by applying +1000 V to the front glass and slowly decreases FF as alkali metal cations gather in the i-ZnO buffer to increase shunt conductance, and (2) p-n junction PID, which results from applying +1000 V to the back glass and rapidly decreases carrier concentration, V_{OC} and FF as alkali metal cations accumulate near the junction. We find that switching from Na-rich SLG to K-rich BSG reduces front shunting PID, and we also find that the standard protocol of stress at SC leads to faster degradation than OC. These results illuminate how PID occurs in CIGS, how to reduce it, and how to test for it.

Acknowledgment

The authors thank Karen Bowers. This work was authored by the National Renewable Energy Laboratory, operated by Alliance for Sustainable Energy, LLC, for the U.S. Department of Energy (DOE) under Contract No. DE-AC36-08GO308. Funding provided by U.S. Department of Energy Office of Energy Efficiency and Renewable Energy (EERE) Solar Energy Technologies Office Award Number 34352. The views expressed in the article do not necessarily represent the views of the DOE or the U.S. Government. The U.S. Government retains and the publisher, by accepting the article for publication, acknowledges that the U.S. Government

Pursuant to the DOE Public Access Plan, this document represents the authors' peer-reviewed, accepted manuscript. The published version of the article is available from the relevant publisher.

retains a nonexclusive, paid-up, irrevocable, worldwide license to publish or reproduce the published form of this work, or allow others to do so, for U.S. Government purposes.

References

Alonso-Garcia, M.C., Hacke, P., Glynn, S., Muzzillo, C.P., Mansfield, L.M., 2019. Analysis of potential-induced degradation in soda-lime glass and borosilicate-glass Cu(In,Ga)Se_2 samples. IEEE J. Photovoltaics 9(1), 331-338.

Boulhidja, S., Mellit, A., Voswinckel, S., 2017. Potential-induced degradation test on CIGS photovoltaic modules, 2017 5th International Conference on Electrical Engineering - Boumerdes (ICEE-B). pp. 1-4.

Boulhidja, S., Mellit, A., Voswinckel, S., Lughi, V., Ciocia, A., Spertino, F., Massi Pavan, A., 2020. Experimental evidence of PID effect on CIGS photovoltaic modules. Energies 13(3), 537-516.

Carolus, J., Breugelmans, R., Tsanakas, J.A., van der Heide, A., Voroshazi, E., De Ceuninck, W., Daenen, M., 2020. Why and how to adapt PID testing for bifacial PV modules? Progress in Photovoltaics: Research and Applications 28(10), 1045-1053.

Colli, A., 2013. The role of sodium in photovoltaic devices under high voltage stress: A holistic approach to understand unsolved aspects. Renewable Energy 60, 162-168.

Contreras, M.A., Hacke, P., Repins, I., 2016. Development of Cu(In, Ga)Se_2 test coupons for potential induced degradation studies, 43rd IEEE Photovoltaic Specialists Conference. pp. 0857-0862.

Fjällström, V., Salomé, P.M.P., Hultqvist, A., Edoff, M., Jarmar, T., Aitken, B.G., Zhang, K., Fuller, K., Williams, C.K., 2013. Potential-induced degradation of $CuIn_{1-x}Ga_xSe_2$ thin film solar cells. IEEE J. Photovoltaics 3(3), 1090-1094.

Fjällström, V., Szaniawski, P., Vermang, B., Salomé, P.M.P., Rostvall, F., Zimmermann, U., Edoff, M., 2015. Recovery after potential-induced degradation of $CuIn_{1-x}Ga_xSe_2$ solar cells with CdS and Zn(O,S) buffer layers. IEEE J. Photovoltaics 5(2), 664-669.

Hacke, P., Terwilliger, K., Glick, S.H., Perrin, G., Wohlgemuth, J.H., Kurtz, S.R., Showalter, K., Sherwin, J.D., Schneller, E., Barkaszi, S., Smith, R.M., 2015. Survey of potential-induced degradation in thin-film modules. J. Photonics Energy 5(1), 14.

Hegedus, S.S., Shafarman, W.N., 2004. Thin-Film Solar Cells: Device Measurements and Analysis. Progress in Photovoltaics: Research and Applications 12(2-3), 155-176.

Hoffmann, S., Koehl, M., 2014. Effect of humidity and temperature on the potential-induced degradation. Progress in Photovoltaics: Research and Applications 22(2), 173-179.

Kambe, M., Hara, K., Mitarai, K., Takeda, S., Fukawa, M., Ishimaru, N., Kondo, M., 2013. PID-free c-Si PV module using aluminosilicate chemically strengthened glass, 28th European Photovoltaic Solar Energy Conference. pp. 2861-2864.

Kapur, J., Stika, K.M., Westphal, C.S., Norwood, J.L., Hamzavytehrany, B., 2015. Prevention of potential-induced degradation with thin ionomer film. IEEE J. Photovoltaics 5(1), 219-223.

Lechner, P., Hummel, S., Geyer, D., Mohring, H.-D., 2013. PID-behaviour of thin-film- and c-Si PV-modules, 28th European Photovoltaic Solar Energy Conference. pp. 2810-2815.

Pursuant to the DOE Public Access Plan, this document represents the authors' peer-reviewed, accepted manuscript. The published version of the article is available from the relevant publisher.

Lechner, P., Sanchez, D., Geyer, D., Mohring, H.-D., 2012. Estimation of time to PID-failure by characterisation of module leakage currents, 27th European Photovoltaic Solar Energy Conference and Exhibition. pp. 3152-3156.
Lee, S., Bae, S., Park, S.J., Gwak, J., Yun, J., Kang, Y., Kim, D., Eo, Y.-J., Lee, H.-S., 2021. Characterization of Potential-Induced Degradation and Recovery in CIGS Solar Cells. Energies 14(15), 4628-4612.
Luo, W., Hacke, P., Hsian, S.M., Wang, Y., Aberle, A.G., Ramakrishna, S., Khoo, Y.S., 2018. Investigation of the impact of illumination on the polarization-type potential-induced degradation of crystalline silicon photovoltaic modules. IEEE J. Photovoltaics 8(5), 1168-1173.
Luo, W., Hacke, P., Terwilliger, K., Liang, T.S., Wang, Y., Ramakrishna, S., Aberle, A.G., Khoo, Y.S., 2018. Elucidating potential-induced degradation in bifacial PERC silicon photovoltaic modules. Progress in Photovoltaics: Research and Applications 26(10), 859-867.
Luo, W., Khoo, Y.S., Hacke, P., Naumann, V., Lausch, D., Harvey, S.P., Singh, J.P., Chai, J., Wang, Y., Aberle, A.G., Ramakrishna, S., 2017. Potential-induced degradation in photovoltaic modules: a critical review. Energy Environ. Sci. 10(1), 43-68.
Mansfield, L.M., Hacke, P., Contreras, M.A., Repins, I.L., 2017. Accelerated PID testing on packaged CIGS devices, Photovoltaic Reliability Workshop.
Mansfield, L.M., Muzzillo, C.P., Glynn, S., Repins, I.L., 2021. Cell-level reliability testing procedures for CIGS photovoltaics. MRS Advances.
Manz, P., Wesselak, V., Voswinckel, S., Trautmann, B., Fokuhl, E., Schmidt, C., 2014. Leakage current pathways and magnitudes in correlation to PID of CIGS thin film modules, 29th European Photovoltaic Solar Energy Conference and Exhibition. pp. 3194-3199.
Moutinho, H.R., Johnston, S., To, B., Jiang, C.S., Xiao, C., Hacke, P., Moseley, J., Tynan, J., Dhere, N.G., Al-Jassim, M.M., 2018. Development of coring procedures applied to Si, CdTe, and CIGS solar panels. Sol. Energy 161, 235-241.
Moutinho, H.R., To, B., Jiang, C.-S., Xiao, C., Muzzillo, C.P., Hacke, P., Moseley, J., Tynan, J., Dhere, N.G., Mansfield, L., Al-Jassim, M.M., Johnston, S., 2018. Artifact-free coring procedures for removing samples from photovoltaic modules for microscopic analysis, 7th World Conference on Photovoltaic Energy Conversion. pp. 1313-1317.
Muzzillo, C.P., Glynn, S., Hacke, P., Moutinho, H.R., Young, M.R., Repins, I.L., Mansfield, L.M., 2019. Potential-Induced Degradation Depends on Leakage Current and Light/Electrical Bias in Cu(In,Ga)Se_2 Devices. IEEE J. Photovoltaics 9(6), 1852-1856.
Muzzillo, C.P., Glynn, S., Hacke, P., Moutinho, H.R., Young, M.R., Teeter, G., Repins, I.L., Mansfield, L.M., 2018. Potential-induced degradation of Cu(In,Ga)Se_2 solar cells: Alkali metal drift and diffusion effects. IEEE J. Photovoltaics 8(5), 1337-1342.
Naumann, V., Geppert, T., Großer, S., Wichmann, D., Krokoszinski, H.-J., Werner, M., Hagendorf, C., 2014a. Potential-induced degradation at interdigitated back contact solar cells. Energy Procedia 55, 498-503.
Naumann, V., Lausch, D., Hähnel, A., Bauer, J., Breitenstein, O., Graff, A., Werner, M., Swatek, S., Großer, S., Bagdahn, J., Hagendorf, C., 2014b. Explanation of potential-induced degradation of the shunting type by Na decoration of stacking faults in Si solar cells. Sol. Energy Mater. Sol. Cells 120, 383-389.

Pursuant to the DOE Public Access Plan, this document represents the authors' peer-reviewed, accepted manuscript. The published version of the article is available from the relevant publisher.

Sakurai, K., Tomita, H., Ogawa, K., Schmitz, D., Shibata, H., Tokuda, S., Masuda, A., 2016. Proposed new damp heat test standards for commercial CIGS modules with bias application or light irradiation. SPIE.
Sakurai, K., Tomita, H., Ogawa, K., Schmitz, D., Shibata, H., Tokuda, S., Masuda, A., 2017. Effect of light irradiation and forward bias during PID tests of CIGS PV modules, SPIE Optical Engineering + Applications. SPIE, pp. 103700C-103703.
Sakurai, K., Tomita, H., Schmitz, D., Tokuda, S., Ogawa, K., Shibata, H., Masuda, A., 2018. Accelerated Outdoor PID Testing of CIGS Modules and Comparison with Indoor PID Tests, 2018 IEEE 7th World Conference on Photovoltaic Energy Conversion (WCPEC). pp. 1320-1323.
Sakurai, K., Tomita, H., Schmitz, D., Tokuda, S., Ogawa, K., Shibata, H., Masuda, A., 2018. Exploring suitable damp heat and potential induced degradation test procedures for Cu(In,Ga)(S,Se) photovoltaic modules. Jpn. J. Appl. Phys. 57(8S3), 08RG02.
Sakurai, K., Tomita, H., Tokuda, S., Schmitz, D., Ogawa, K., Shibata, H., Masuda, A., 2019. Rapid Recovery of CIGS Solar Cells from PID Stress with Light Soaking, 2019 IEEE 46th Photovoltaic Specialists Conference (PVSC). pp. 2000-2002.
Salomon, O., Hempel, W., Kiowski, O., Lotter, E., Witte, W., Ferati, A., Schneikart, A., Kaune, G., Schäffler, R., Becker, M., Schröppel, B., Vidal Lorbada, R., Mücke, D., Walter, T., 2019. Influence of molybdenum back contact on the PID effect for Cu(In,Ga)Se_2 solar cells. Coatings 9(12), 794-712.
Schulze, A., Koentopp, M.B., Taubitz, C., 2020. A drift and diffusion model for PID-s in solar modules. IEEE J. Photovoltaics 10(5), 1403-1408.
Swanson, R., Cudzinovic, M., DeCeuster, D., Desai, V., Jürgens, J., Kaminar, N., Mulligan, W., Rodrigues-Barbarosa, L., Rose, D., Smith, D., 2005. The surface polarization effect in high-efficiency silicon solar cells, 15th International Photovoltaic Science and Engineering Conference. Shanghai, China, pp. 410-413.
Theelen, M., Daume, F., 2016. Stability of Cu(In,Ga)Se_2 solar cells: A literature review. Sol. Energy 133, 586-627.
Vermang, B., Rostvall, F., Fjällström, V., Edoff, M., 2014. Potential-induced optimization of ultra-thin rear surface passivated CIGS solar cells. Phys. Status Solidi RRL 8(11), 908-911.
Voswinckel, S., Mikolajick, T., Wesselak, V., 2020. Influence of the active leakage current pathway on the potential induced degradation of CIGS thin film solar modules. Sol. Energy 197, 455-461.
Walter, T., 2015. Chapter three - Reliability issues of CIGS-based thin film solar cells, in: Willeke, G.P., Weber, E.R. (Eds.), Semiconductors and Semimetals. Elsevier, pp. 111-150.
Weber, T., Berghold, J., Heilmann, F., Roericht, M., Krauter, S., Grunow, P., 2013. Test sequence development for evaluation of potential induced degradation on thin-film modules, 28th European Photovoltaic Solar Energy Conference. pp. 3324-3331.
Weber, T., Hinz, C., Leers, M., Grunow, P., Podlowski, L., 2017. A review of potential induced degradation in thin-film plants, 33rd European Photovoltaic Solar Energy Conference and Exhibition. pp. 1671-1676.
Xiao, C., Jiang, C., Harvey, S.P., Mansfield, L., Muzzillo, C.P., Sulas, D., Liu, J., Johnston, S., Al-Jassim, M., 2019. In-situ microscopy characterization of Cu(In,Ga)Se_2 potential-induced degradation, 2019 IEEE 46th Photovoltaic Specialists Conference. pp. 2342-2345.

Pursuant to the DOE Public Access Plan, this document represents the authors' peer-reviewed, accepted manuscript. The published version of the article is available from the relevant publisher.

Xiong, Z., Walsh, T.M., Aberle, A.G., 2011. PV module durability testing under high voltage biased damp heat conditions. Energy Procedia 8, 384-389.
Yamaguchi, S., Jonai, S., Hara, K., Komaki, H., Shimizu-Kamikawa, Y., Shibata, H., Niki, S., Kawakami, Y., Masuda, A., 2015. Potential-induced degradation of Cu(In,Ga)Se_2 photovoltaic modules. Jpn. J. Appl. Phys. 54(8S1), 08KC13.
Yilmaz, P., Schmitz, J., Theelen, M., 2022. Potential induced degradation of CIGS PV systems: A literature review. Renewable Sustainable Energy Rev. 154, 111819.

Pursuant to the DOE Public Access Plan, this document represents the authors' peer-reviewed, accepted manuscript. The published version of the article is available from the relevant publisher.